Neurotherapeutics (2021) 18:2107–2125
https://doi.org/10.1007/s13311-021-01092-9

ORIGINAL ARTICLE

Donepezil Protects Against Doxorubicin-Induced Chemobrain in Rats via Attenuation of Inflammation and Oxidative Stress Without Interfering With Doxorubicin Efficacy

Benjamin Ongnok[1,2,3] · Thawatchai Khuanjing[2,3] · Titikorn Chunchai[1,2,3] · Patcharapong Pantiya[1,2,3] · Sasiwan Kerdphoo[1,3] · Busarin Arunsak[1,3] · Wichwara Nawara[1,3] · Thidarat Jaiwongkam[1,3] · Nattayaporn Apaijai[2,3] · Nipon Chattipakorn[1,2,3] · Siriporn C. Chattipakorn[1,2,4]

Accepted: 10 July 2021 / Published online: 26 July 2021

Summary

Although doxorubicin (Dox) is an effective chemotherapy medication used extensively in the treatment of breast cancer, it frequently causes debilitating neurological deficits known as chemobrain. Donepezil (DPZ), an acetylcholinesterase inhibitor, provides therapeutic benefits in various neuropathological conditions. However, comprehensive mechanistic insights regarding the neuroprotection of DPZ on cognition and brain pathologies in a Dox-induced chemobrain model remain obscure. Here, we demonstrated that Dox-treated rats manifested conspicuous cognitive deficits and developed chemobrain pathologies as indicated by brain inflammatory and oxidative insults, glial activation, defective mitochondrial homeostasis, increased potential lesions associated with Alzheimer's disease, disrupted neurogenesis, loss of dendritic spines, and ultimately neuronal death through both apoptosis and necroptosis. Intervention with DPZ co-treatment completely restored cognitive function by attenuating these pathological conditions induced by DOX. We also confirmed that DPZ treatment does not affect the anti-cancer efficacy of Dox in breast cancer cells. Together, our findings suggest that DPZ treatment confers potential neuroprotection against Dox-induced chemobrain.

Keywords Chemotherapy · Chemobrain · Neurotoxicity · Doxorubicin · Donepezil · Acetylcholinesterase inhibitor

Introduction

Although the incidence of cancer occurrence is increasing worldwide [1], cancer survivor rates have been expected to continue to improve due to advancements in medical diagnosis and treatments [2]. Chemotherapeutic agents have been considered to be one of the most successful therapeutic procedures against various types of cancer. Unfortunately, chemotherapy carries a vast number of debilitating side effects provoked by its cytotoxic properties, including chronic neurocognitive deficits. There is growing evidence to suggest that up to 70% of cancer survivors with a history of chemotherapy treatment develop cognitive impairment in several cognitive domains [3–6]. Hence, cognitive status is a critical criterion for assessing therapeutic outcomes potentially limiting dosage administration in clinical settings. The neurological consequences during or following chemotherapy are referred to as chemotherapy-induced cognitive impairment (CICI), colloquially known as "chemobrain" [7, 8].

Over the past 20 years, chemobrain has been prevalent among numerous breast cancer survivors whose predominant chemotherapeutic treatment was doxorubicin (Dox) [4, 9]. Even though the passage of Dox through the blood–brain barrier (BBB) is limited, Dox induces the release of tumor necrosis factor-alpha (TNF-α) through the oxidation of plasma-resident ApoA1, which in turn crosses the BBB via receptor-mediated endocytosis and enters the brain. The

✉ Siriporn C. Chattipakorn
siriporn.c@cmu.ac.th

1 Cardiac Electrophysiology Research and Training Center, Faculty of Medicine, Neuroelectrophysiology Unit, Chiang Mai University, 50200, Chiang Mai, Thailand

2 Center of Excellence in Cardiac Electrophysiology Research, Chiang Mai University, 50200, Chiang Mai, Thailand

3 Cardiac Electrophysiology Unit, Department of Physiology, Chiang Mai University, 50200, Chiang Mai, Thailand

4 Department of Oral Biology and Diagnostic Sciences, Faculty of Dentistry, Chiang Mai University, 50200, Chiang Mai, Thailand

ligation of TNF-α with the tumor necrosis factor receptors (TNFRs) can augment neuroinflammation by enhancing the activation of microglia and astrocytes which contribute to a massive release of pro-inflammatory cytokines and the production of reactive oxygen species (ROS) in the brain [10–12]. Therefore, neuroinflammation caused by glial activation is presumed to be the pathogenetic mechanism associated with Dox-induced chemobrain, eventually culminating in neuronal death and brain function deterioration.

Mitochondrial dysfunction is also implicated in several neurodegenerative diseases [13]. Pertinent to chemobrain, Dox injection disturbed mitochondrial function in the brain, as established by increased brain mitochondrial ROS levels and impaired mitochondrial respiratory capacity [14, 15]. Previous studies demonstrated that elevated TNF-α levels play a central role in underlying mitochondrial dysfunction in the brain following Dox administration, further emphasizing the impact of neuroinflammation in Dox-induced chemobrain [15, 16].

It has also been recognized that neuroinflammation creates pathological microenvironments which in turn perturb the physiological regulation of adult hippocampal neurogenesis. There is a weight of evidence to support the activation of microglia and astrocytes during an inflammatory episode disrupts the proliferation and survival of new neuronal cells [17]. A recent study similarly demonstrated that the reduction of brain-derived neurotrophic factor (BDNF) and tropomyosin receptor kinase B (TrkB) partly orchestrated the loss of the newly proliferating neurons in the hippocampus, contributing to the impairment of spatial and working memory following Dox administration [14]. For these reasons, the neurogenic symptoms associated with chemotherapy are largely localized to the hippocampus, the area responsible for the consolidation of long-term memory [18].

With regard to the roles of the cholinergic system in physiological brain functioning, the dysregulation of cholinergic activity is a major hallmark of many neurodegenerative diseases, including Alzheimer's disease (AD) [19]. Donepezil, an acetylcholinesterase (AChE) inhibitor, is extensively used to attenuate the psychiatric and cognitive symptoms of AD by sustaining synaptic acetylcholine (ACh) levels and prolonging the activation of ACh receptors (AChRs), thus improving cognitive function in AD patients [20]. One of our previous studies has also shown that DPZ treatment exerted pleiotropic effects including anti-inflammatory and antioxidant properties in a model of brain damage resulting from cardiac ischemia/reperfusion injury [21]. However, much of the existing knowledge regarding the pathophysiology of Dox-induced chemobrain remains diffuse, and the potential protection by cholinergic enhancement is currently unsubstantiated. We thus sought to investigate the therapeutic actions of cholinergic activation on neuropathology in rats with Dox-induced chemobrain by using DPZ. Of critical interest, the present study also confirmed that DPZ itself did not affect the therapeutic efficacy of Dox in breast cancer cells. The study therefore provides important knowledge to clarify possible mechanisms associated with DOX-induced cognitive deficits and paves the way toward using AChE inhibitors as a novel strategy for the treatment or prevention of chemobrain in cancer patients.

Methods

Animal Model

All animal experiments were carried out in accordance with the approved protocol by the Institutional Animal Care and Use Committee of Chiangmai University (Permit Number: 2563/RT-0012) and within the guidelines established by NIH (*Guide for the care and use of laboratory animals*). Male Wistar rats (n = 24, 350–400 g, 8 weeks old) were obtained from the Nomura Siam International Co., Ltd., Bangkok, Thailand. The animals were individually housed at laboratory animal center of Chiangmai University in a temperature-controlled environment with a 12h light:dark cycle with ad libitum access to food and water. All rats were blindly randomized into 3 groups to receive different treatments: (1) Control group: given 0.9% normal saline solution; (2) Dox group: given doxorubicin; (3) Dox + DPZ group: co-treated with doxorubicin and donepezil.

In this study, we used eight animals/group for the cognitive assessment. At the end of the experimental protocol, all rats were euthanized and the brain tissues from each group were removed for further investigation as shown in Supplementary Fig. 1A. The cortices from each group were dissected and separated to determining brain oxidative stress, reverse transcription-quantitative PCR (RT-qPCR), and brain mitochondrial function. The left hippocampal tissue was isolated from cortex on ice and kept at − 80 °C for western blotting analysis. The right hippocampus from each animal was fixed in 4% paraformaldehyde for the fluorescent staining of dendritic spine, microglia, and astrocyte.

Chemotherapy and Treatment Paradigm

To develop the chemobrain model, Dox dissolved in saline (3 mg/kg; Fresenius Kabi Oncology Ltd., India) was intraperitoneally injected (i.p.) for 6 doses. The first 3 doses were injected into rats every 4 days, followed by the final 3 doses injected once a week. DPZ (5 mg/kg; Sigma-Aldrich, USA) was dissolved in sterile water and administered via oral gavage daily for 30 consecutive days, beginning at the same times as the first Dox injection. The experimental protocol is summarized in Supplementary Fig. 1B.

Behavioral Test

Open-Field Test (OFT)

The OFT was performed to evaluate anxiety and general locomotive activity in rodents. In this assessment, an applied apparatus was used which consisted of a circular-based box open from above (70 cm of diameter, 50 cm of height). Each rat was placed at the center of the arena and allowed 10 min for exploring. Time spent in the center, total distance, and average speed were recorded through the camera and analyzed using the Smart version 3 program. These parameters were evaluated to exclude different locomotor activity among groups.

Modified Novel Object Location Test (NOL) and Novel Object Location Test (NOR)

The NOL and NOR were included to assess long-term learning and memory. The tests were modified so that the NOL was performed followed by the NOR with a 24 h interval resting period [22, 23]. In brief, during the habituation phase, the rats were placed into the center of the apparatus and left for 10 min. They were then removed. After 24 h, each rat was placed at the same point in the apparatus and allowed to explore two identical objects for 10 min in a familiarization phase. On the next day, rats were placed into the apparatus containing two familiar objects, but one object was placed at the opposite end from the previous location. The rats were left for 10 min. The percentage preference index was estimated from the following formula: % index preference = [(time on the object with new location) ÷ (time on object at same location + time on the object with new location)] × 100. After 24 h, rats were placed into the box containing one familiar object placed at the same location, and one novel object placed at the opposite end from the familiar object. The rats were allowed to explore for 10 min. The time interacting with new objects was recorded and represented as the % preference index calculated from the following formula: % index preference = [(time on the novel object) ÷ (time on familiar object + time on the novel object)] × 100.

RT-qPCR Analysis

Briefly, the frozen brain tissues in RNA*later*™ stabilizing solution were homogenized in a Mini-BeadBeater with 1 mm sterile zirconia/silica bead (Biospec Products, USA). Total RNA extractions from brain tissues were isolated using the Trizol (Thermo Fisher Scientific, USA) method according to the manufacturer's instructions. The concentrations of mRNA products were evaluated using the Take3 microvolume plate (BioTek Instruments, Inc., USA). An optical density at a wavelength of 260/280 nm range of 1.8–2.0 was chosen to indicate the purification of mRNA. Then, single-stranded complementary DNA (cDNA) was synthesized from 2000 ng of purified mRNA using an iScript cDNA synthesis kit (Bio-Rad Laboratories Ltd.). cDNA concentrations were measured and diluted to 100 ng/µl in RNase-free H_2O. All cDNA samples were subjected to quantitative PCR performed on the Bio-Rad Cx96 Detection System (Bio-Rad Laboratories Ltd., USA) using the SsoFast™ EvaGreen supermix kit (Bio-Rad Laboratories Ltd., USA). The final volume for each reaction was 20 µl with 2 µl of cDNA sample and 10 µM of forward and reverse gene-specific primers. Forty-cycle amplification, 5 s at 95 °C for denaturation, and 10 s at 55 °C for annealing were performed for each gene. Relative quantitation of the mean Ct values for the PCR product was normalized to *β-actin* as an internal standard. The sequences of gene-specific primers are listed in Table 1.

Determination of Brain Malondialdehyde (MDA) Level

A high-performance liquid chromatography (HPLC)-based assay was used to measure the brain tissue levels of MDA [24]. Protein lysate extracted from the brain tissue was precipitated with 10% (w/v) trichloroacetic acid (TCA) and heated at 90 °C for 30 min. The mixture was then centrifuged at 6,000 rpm for 10 min. Then, the supernatant was further incubated with 0.44 M H_3PO_4 and 0.6% thiobarbituric acid (TBA) at 90 °C for 30 min. The concentrations of thiobarbituric acid-reactive substrates (TBARS) were determined at a wavelength of 532 nm using an HPLC system. A standard curve was constructed from the area under the curve of serial 1, 1, 3, 3-tetramethoxypropane concentrations. Brain TBARS concentrations were quantified directly from a standard curve and reported as MDA equivalent concentration [25].

Determination of the Morphology of Microglia and Astrocytes by Immunofluorescence Labeling

After decapitation, the brains were post-fixed in 4% paraformaldehyde overnight at room temperature prior to cryoprotection in 30% sucrose in PBS at 4 °C until further tissue

Table 1 The sequences of gene-specific primers used in the study

Gene	Forward primer (5′–3′)	Reverse primer (5′–3′)
Tnfa	ACTCCCAGAAAAGCAAGCAA	CGAGCAGGAATGAGAAGAGG
Il6	TCCTACCCCAACTTCCAATGCTC	TTGGATGGTCTTGGTCCTTAGCC
β-actin	GGAGATTACTGCCCTGGCTCCTA	GACTCATCGTACTCCTGCTTGCTG

preparation. The brains were sectioned at 20 µm thickness by cryosectioning (Leica CM1950, Germany). Sections were quenched with 3% H_2O_2 solution and 0.2% Triton X-100 in distilled water for 1 h and then blocked with 5% BSA in PBS for 1 h at room temperature. The brain slices were further incubated overnight with a primary antibody against Iba-1 or GFAP to probe microglia and astrocytes, respectively. The following day, sections were rinsed with PBS and incubated in AlexaFluor conjugated secondary antibodies (1:1000) including Iba1-AlexaFluor 488 anti-goat IgG and GFAP-AlexaFluor 647 anti-rabbit IgG, for 1 h at 25 °C followed by staining with DAPI (1:500; TOCRIS, Bristol, UK). Sections were washed with PBS and mounted with the anti-fading mounting medium (Sigma-Aldrich Chemie, Germany). The z-stacks of microglial and astrocyte images at CA1 of the hippocampus were acquired using a confocal microscope (Olympus FLUOVIEW FV3000, Japan). Microglial and astrocyte morphology were analyzed as previously described [26]. The complexities of microglia and astrocyte were evaluated using Sholl analysis [27–29]. In brief, the 3D morphology structure was constructed using the filament mode of the Imaris software. The center of the soma was traced by a series of concentric circles to signify the beginning point of the analysis. Ten-micrometer increment steps were set as the Sholl radius and the intersection numbers between cell process and the radius were automatically counted by the software. To construct a graph to represent the Sholl analysis, the intersection numbers were plotted against the radial distance from the soma. The area under the curve (AUC) of the intersection was further determined from the AUC in the intersection number graph. The higher AUC indicated the higher complexity of microglia and astrocyte.

Brain Mitochondrial Status

After decapitation, the brain was rapidly removed and the blood was washed out with 5 ml of ice-cold MSE solution (1 mg/ml bovine serum albumin (BSA), 225 mM mannitol, 75 mM sucrose, 5 mM HEPES, 1 mM EGTA, pH 7.4). Then, the brain was transferred into 10 ml of 0.05% bacterial proteinase bacterial (Sigma, USA) in ice-cold MSE solution and homogenized at 600 rpm. After that, the brain mitochondrial fraction was isolated by differential centrifugation as described in our previous study [30]. Mitochondrial protein concentration was measured by bicinchoninic acid assay adjusting for concentration of 0.4 mg/ml [31]. The brain mitochondrial fraction was used to evaluate mitochondrial status including brain mitochondrial ROS level, mitochondrial membrane potential change ($\Delta\Psi m$), and mitochondrial swelling. To ascertain mitochondrial ROS production, the mitochondrial fraction was incubated with 2 µM 2′-7′dichlorofluorescin diacetate (DCFH-DA) fluorescent dye. The fluorescence intensity of dichlorofluorescein (DCF) was detected with excitation/emission wavelengths of 485 nm/535 nm. Brain mitochondrial membrane potential changes were determined by staining isolated mitochondria with JC-1 fluorescent dye. A reduction of red (JC-1 polymer) to green (JC-1 monomer) fluorescence ratio indicates the mitochondrial membrane depolarization. Finally, swelling of brain mitochondria was studied using the absorbance of mitochondrial suspension at a wavelength of 540 nm. A decrease in the mitochondrial suspension absorbance indicated mitochondrial swelling. All measurements were detected using a microplate reader (Gen5 Microplate Reader, BioTek Instruments, VT, USA).

Western Blot Analysis

After decapitation, the hippocampus was rapidly isolated on ice and immediately frozen in liquid nitrogen. The hippocampal tissues were homogenized with a non-ionizing lysis buffer containing 1 × protease inhibitor. The concentration of total protein was determined using a Bradford protein assay (Bio-Rad Laboratories, USA). The tissue lysates were electrophoresed on 10% or 12.5% sodium dodecyl sulfate–polyacrylamide gel electrophoresis (SDS-PAGE) and transferred to a nitrocellulose membrane. The membranes were incubated in blocking solution (5% BSA, 0.1% Tween 20 in Tris-buffer saline; TBST, pH7.4) at room temperature for 1 h. All immunoblots were subsequently probed with primary antibodies including anti-GPx4, anti-SOD2, anti-DRP1, anti-p-DRP1^{Ser616}, anti-OPA1, anti-Mfn1, anti-Mfn2, anti-Parkin, anti-Beclin-1, anti-p62, anti-Amyloid-β, anti-APP, anti-BACE-1, anti-p-Tau, anti-Tau, anti-RAGE, anti-BDNF, anti-TrkB, anti-p-TrkB^{Tyr515}, anti-DCX, anti-PSD95, anti-Bax, anti-Bcl-2, anti-Caspase-3, anti-p-RIP1, anti-RIP1, anti-p-MLKL, anti-MLKL, and anti-β-Actin. After washing 3 times with TBST, immunodetection was performed via co-incubation with horseradish peroxidase-conjugated secondary antibodies for 1 h. Immunoreactivities of the protein bands were enhanced using Clarity™ Western ECL Blotting Substrate (Bio-Rad Laboratories, USA) and visualized using the ChemiDoc™ Touch Gel Imaging System. The densitometric analysis of the bands was carried out using Image J (NIH image) analysis software.

Dendritic Spine Staining

For visualization of dendritic spines, the brains were sliced with a vibratome to 400 nm of thickness. Slices were fixed in 4% paraformaldehyde and were stained via juxtacellular labeling with the carbocyanine dye 1,1′-dioctadecyl-3,3,3′,3′-Tetramethylindocarbocyanine Perchlorate (DiI; Invitrogen, Oregon, USA). Slices were incubated with DiI solution for 7 days before being mounted on slides with PBS. The secondary or tertiary dendritic segments at CA1 region were captured using a confocal microscope (Olympus

FLUOVIEW FV3000, Japan) with 0.25 mm in the z-plane. For quantitative spine analysis, three neuronal cells per brain slice and three brain slices per animal were used to randomly measure dendritic spine density and volume [32]. The dendritic spine density and spine volume were determined using Imaris software (Oxford Instruments).

Cell Culture

Breast cancer cell lines including MCF-7 (low metastatic potential) and MDA-MB-231 (high metastatic potential) were chosen to represent different phenotypes of this heterogeneous disease. The cells were cultured in Dulbecco's Modified Eagle Medium/Nutrient Mixture F-12 (DMEM/F-12) supplemented with 10% fetal bovine serum, 1% antibiotic solution (100 U/mL of penicillin and 100 mg/mL of streptomycin), and incubated in a humidified atmosphere of 5% CO_2 in air at 37 °C. An MTT assay (Invitrogen, Oregon, USA) was used to evaluate the percentage of cell viability. Briefly, 5×10^3 cells were seeded into a 96-well plate in triplicate and then incubated for 24 h. The cells were then treated with Dox at a concentration of 0.3125 µM and/or gradient concentrations of DPZ including 0.5, 1, and 2 µM for 48 h. After the treatments, the medium was replaced with 100 µL of fresh culture medium and 15 µL of 12 mM of MTT solution was added to each well. Four hours later, the violet formazan product within metabolically viable cells was solubilized with 100 µL of DMSO. The absorbance of formazan crystals was read at 540 nm using a microplate reader. % cell viability was calculated as (mean OD of the testing well ÷ mean OD of the control well) × 100. All experiments were performed on exponentially growing cells.

Quantification and Statistical Analysis

All data of each experiment were expressed as mean ± SEM and processed using GraphPad Prism software (version 7, GraphPad Software, Inc., CA, USA). A one-way ANOVA followed by an LSD post hoc test was performed to compare the differences between groups. A p value of < 0.05 was considered as a measure of statistical significance.

Results

DPZ Alleviated Cognitive Impairment in Rats with Dox-Induced Chemobrain

Since motor and anxiety-like behaviors could impact the results of cognitive assessment, we first evaluated the modulatory effects of our treatments on locomotor activity and anxiety throughout the experiment using an OFT. To determine cognitive behavior, we evaluated long-term learning and memory using a modified NOL test and NOR test. The NOR test was carried out 24 h after NOL to confirm the results and to calibrate the tests for long-term cognitive function. The procedures used in the cognitive tests are shown in Fig. 1a. There were no significant differences between all groups in the total distance traveled, average speed, and total time spent in the central zone, indicating no potential impact of any motor disorders and anxiety on cognitive assessments (Fig. 1b–d). During the familiarization phase, an equal preference index for two objects was observed in all groups, indicating no preference between them (Fig. 1d). The Dox group showed an impairment in spatial memory as represented by a significant decrease in preference index in the NOL phase, compared with that of the control group ($p < 0.05$; Fig. 1f). Dox-treated rats also showed a deficit in the ability to discriminate between the novel and familiar objects in the NOR phase, in comparison to NSS-treated rats (control group) ($p < 0.05$; Fig. 1g). Interestingly, DPZ co-treatment significantly improved the preference indices of both NOL and NOR tests relative to those observed in the Dox group ($p < 0.05$; Fig. 1f and g). Collectively, these findings demonstrated that the administration of DPZ improved long-term learning and memory in rats with Dox-induced chemobrain.

DPZ Reduced Neuroinflammation and Brain Oxidative Stress in Rats with Dox-Induced Chemobrain

We determined the expression of the mRNA of inflammatory cytokines (TNF-α and IL-6) and brain MDA levels. As expected, the quantitative PCR analysis revealed that Dox administration significantly upregulated gene expression of TNF-α and IL-6, which were restored by DPZ co-treatment ($p < 0.05$; Fig. 2a and b). Furthermore, brain MDA levels were significantly higher in the Dox group than those of the control group, indicating an oxidative burst in the brain following Dox administration ($p < 0.05$; Fig. 3a and b). Importantly, treatment with DPZ effectively ameliorated brain oxidative stress in Dox-treated rats by decreasing MDA levels in the brain tissues ($p < 0.05$; Fig. 2c). Hippocampal glutathione peroxidase 4 (GPx4) expression was significantly increased in both the Dox and Dox + DPZ groups, when compared with the controls ($p < 0.05$; Fig. 2d). These findings might be due to the compensatory effect against Dox-induced oxidative stress. However, the expression of superoxide dismutase 2 (SOD2) level did not differ between groups (Fig. 2e).

DPZ Attenuated Glial Morphological Changes in Rats with Dox-Induced Chemobrain

The activation of glial cells in the brain is considered key to the pathogenesis of several neurodegenerative diseases as this

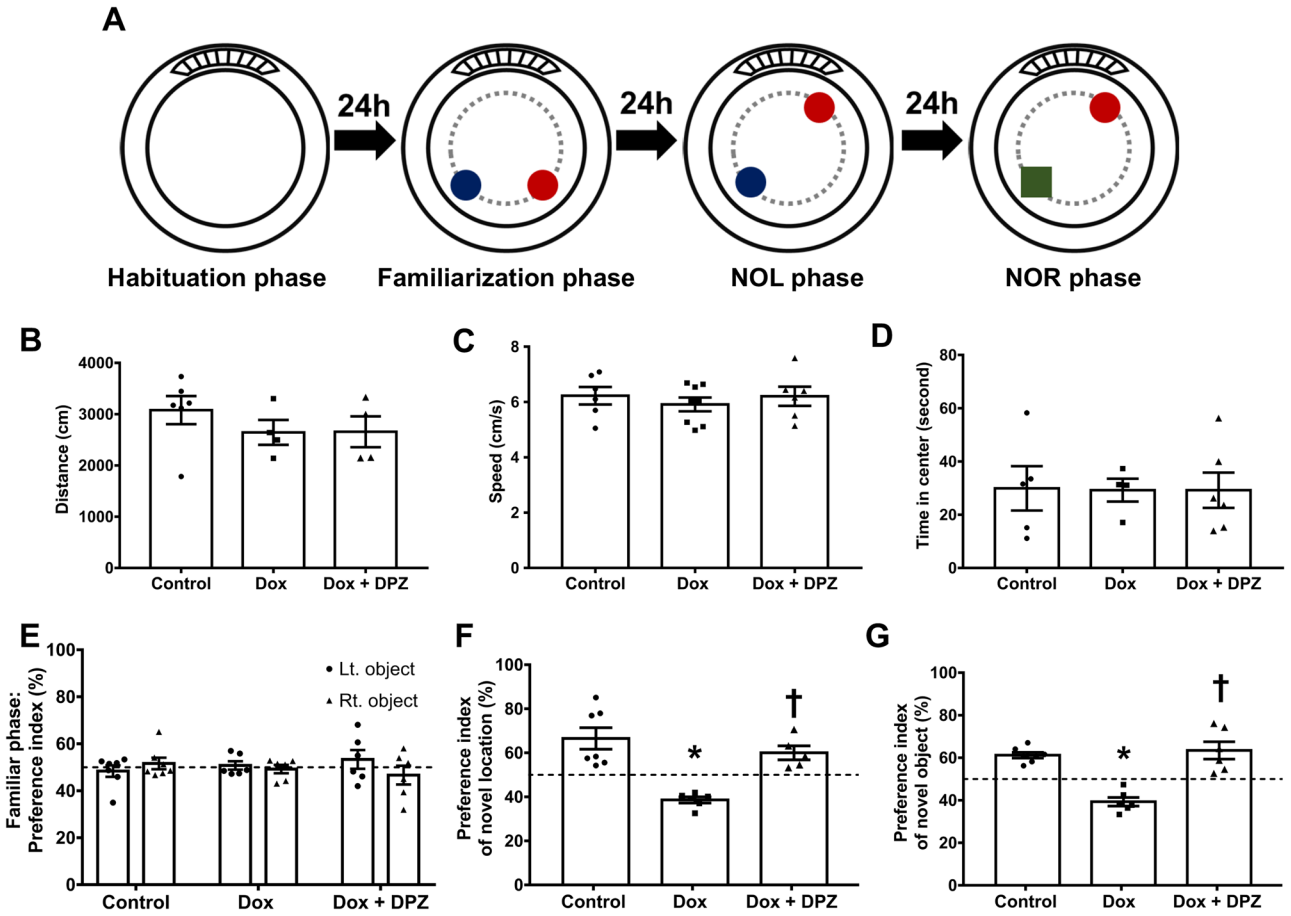

Fig. 1 The effects of donepezil on locomotion, anxiety, and cognition in rats with doxorubicin-induced chemobrain. **A** The behavioral test procedure. **B** The total distance traveled in the open-field test. **C** The average speed traveled in the open-field test. **D** The total time spent in the center of the open-field apparatus. **E** The percentage preference index of two objects during the familiar phase in modified novel object location and recognition tests. **F** The percentage preference index of the object in a novel location during the novel object location test. **G** The percentage preference index of a novel object during the novel object recognition test. The Gaussian distribution was tested using the Shapiro–Wilk normality test for (**E–G**). $n = 6–8$/group; * $p < 0.05$ vs. Control; † $p < 0.05$ vs. Dox (one-way ANOVA followed by an LSD post hoc test). Dox, doxorubicin; DPZ, donepezil; NOL, novel object location test; NOR, novel object recognition test; OFT, open-field test

activation causes neuroinflammation and oxidative stress. To investigate this, microglial and astrocyte activation was morphologically assessed. Representative microglial and astrocyte morphologies from the hippocampal CA1 area of each group are shown in Figs. 3a and 4a. An analysis using Imaris software showed that the number, mean fluorescent intensity, and soma volume of Iba1 positive cells were all significantly increased in the Dox group, when compared to the control group ($p < 0.05$; Fig. 3b–d). The changes in the dendritic branch levels of microglial processes are represented in Fig. 3e. Dox-treated rats exhibited less complex and less branched microglia as indicated by a significantly decreased process length and area under the curve of Iba-1 intersections ($p < 0.05$; Fig. 3f–h), when compared to the control group. Interestingly, DPZ treatment preserved all microglial parameters to a degree equal to those observed in the hippocampus of the control group ($p < 0.05$; Fig. 3b–h).

In addition to microglia, significant increases in the number, mean fluorescent intensity, and soma volume of GFAP positive cells from Dox-treated rats were observed when compared with the controls ($p < 0.05$; Fig. 4b–d). Filament analysis of astrocyte processes also revealed differences in dendritic branch levels in each group as shown in Fig. 4e. The ramifications of the astrocytes from the Dox group were markedly reduced, as indicated by decreasing process length and area under the curve of GFAP intersections ($p < 0.05$; Fig. 4f–h). All changes in astrocyte morphology were restored by DPZ treatment to a level of statistical significance ($p < 0.05$; Fig. 4b–h). All of these results suggest that Dox administration induced microglial and astrocyte morphological changes into the amoeboid-shaped phenotype, implying the hyperactivation of glial cells in the hippocampus of rats. These alterations in microglial and astrocyte morphology were attenuated by DPZ treatment.

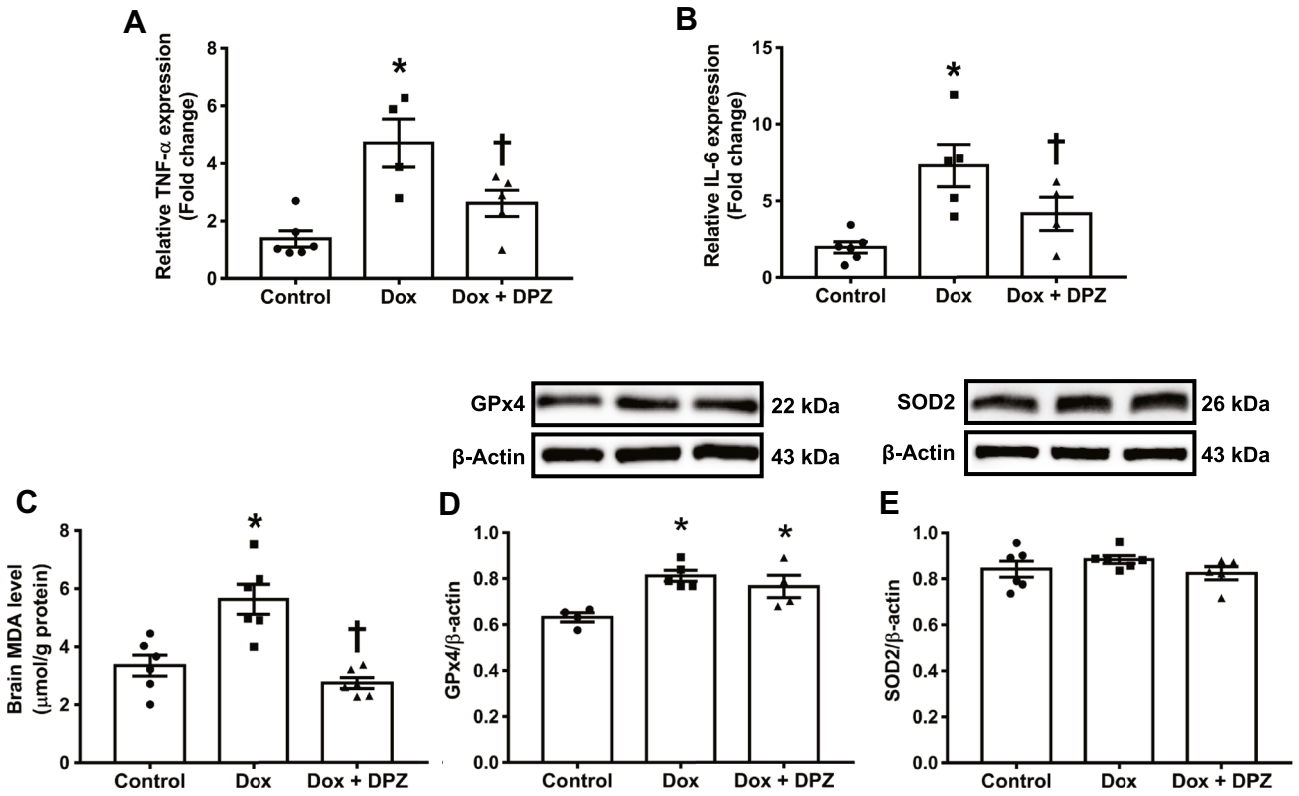

Fig. 2 The effects of donepezil on neuroinflammation and oxidative stress in rats with doxorubicin-induced chemobrain. **A** TNF-α mRNA expression. **B** IL-6 mRNA expression. **C** Brain MDA levels. **D** GPx4 protein expression. **E** SOD2 protein expression. $n = 4$–6/group; * $p < 0.05$ vs. Control; † $p < 0.05$ vs. Dox (one-way ANOVA followed by an LSD post hoc test). Dox, doxorubicin; DPZ, donepezil. GPx4, glutathione peroxidase 4; IL-6, interleukin-6; SOD2, superoxide dismutase 2; TNF-α, tumor necrosis factor-α

DPZ Improved Mitochondrial Status and Attenuated Disturbance of Brain Mitochondrial Dynamics, Mitophagy, and Autophagy in Rats with Dox-Induced Chemobrain

The status of brain mitochondria including the level of ROS production, membrane potential change, and mitochondrial swelling was also investigated. Our results showed that brain mitochondrial ROS production was substantially increased in Dox-treated rats as indicated by an increase in the percentage increase in brain mitochondrial ROS production after H_2O_2 stimulation, compared to the control group ($p < 0.05$; Fig. 5a). Additionally, Dox-treated rats had verifiable mitochondrial membrane depolarization as represented by a marked increase in H_2O_2-stimulated membrane potential changes, compared with the control group ($p < 0.05$; Fig. 5b). Furthermore, the Dox group showed brain mitochondrial swelling, as represented by a substantial decrease in the absorbance of the mitochondrial fraction, compared to the control group ($p < 0.05$; Fig. 5c). Dox-induced brain mitochondrial defects were completely reversed by DPZ co-treatment ($p < 0.05$; Fig. 5a–c). The expression of proteins related to mitochondrial dynamics was additionally evaluated. The Dox group exhibited a significant increase in the ratio of the expression of phosphorylated Drp-1 at serine 616 to total form of Drp-1 (p-Drp-1^{Ser616}/Drp-1) in comparison to the control group, indicating an upregulation of the mitochondrial fission process ($p < 0.05$; Fig. 5d and e). Notably, DPZ-treated rats had a substantially reduced p-Drp-1^{Ser616}/Drp-1 expression ratio, when compared with Dox-treated rats ($p < 0.05$; Fig. 5d and e). Surprisingly, it was found that both Dox and DPZ treatments enhanced mitochondrial fusion as confirmed by increased levels of Mfn1, Mfn2, and OPA1 relative to those observed in the control group ($p < 0.05$; Fig. 5d and f–h). These findings suggest that Dox caused mitochondrial dysfunction and mitochondrial dynamic imbalance in the brain, and the administration of DPZ alleviated mitochondrial fission, while preserving mitochondrial fusion.

The clearance of dysfunctional mitochondria from the fission process is carried out by mitophagy. Therefore, we determined the expression of Parkin protein (marker of mitophagy). The results demonstrated that Dox administration led to an upregulation of the mitophagy process as represented by increased Parkin expression in comparison with the control group, and DPZ co-treatment restored the

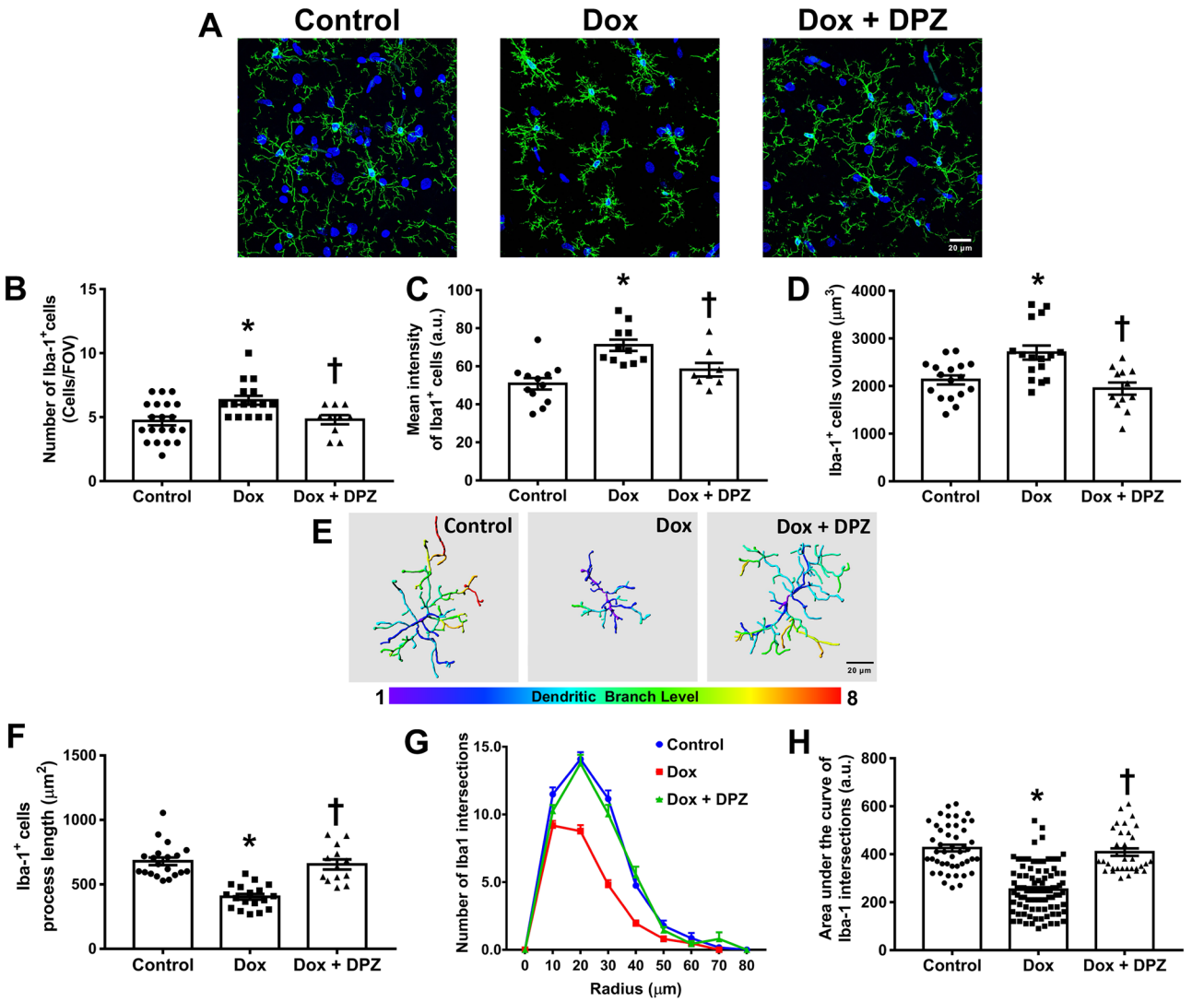

Fig. 3 The effects of donepezil on microglial morphology in rats with doxorubicin-induced chemobrain. **A** Representative images of Iba-1 immunofluorescence under confocal microscopy at CA1 of the hippocampus. **B** The number of Iba-1 positive cells. **C** Mean intensity of Iba-1 positive cells. **D** Soma volume of Iba-1 positive cells. **E** Representative branch level of microglial processes. **F** Process length of Iba-1 positive cells. **G** Microglial process complexity as the number of Iba-1 positive cell process intersections using Sholl analysis. H Representative area under the curve of Sholl analysis. $n = 12$ slices from 6 rats/group; * $p < 0.05$ vs. Control; † $p < 0.05$ vs. Dox (one-way ANOVA followed by an LSD post hoc test); Dox, doxorubicin; DPZ, donepezil; FOV, field of vision

expression of Parkin to the control level ($p < 0.05$; Fig. 5d and i). Additionally, our results showed that the expression of beclin-1 level was markedly downregulated in the Dox group, compared to the control group ($p < 0.05$; Fig. 5d and j). An increased expression of p62 was observed in Dox-treated rats when compared with the control group, indicating a blockage of autophagic flux following Dox treatment ($p < 0.05$; Fig. 5d and k). Importantly, DPZ effectively reversed the disruption of the brain autophagic process indicated by increased beclin-1 and decreased p62 expression, compared with the Dox group ($p < 0.05$; Fig. 5d and i–k).

DPZ Attenuated Potential Lesions of AD and Restored Neurogenesis in Rats with Dox-Induced Chemobrain

To investigate expression levels of AD-associated proteins following Dox administration, western blot analysis was used to determine the expression levels of AD-related proteins (Aβ, APP, BACE, Tau, and p-Tau), and the brain aging marker RAGE. The expression ratio of Aβ/APP was markedly decreased in the Dox group in comparison to the control group, indicating potential amyloid lesions ($p < 0.05$; Fig. 6a and b). Dox-treated rats consistently

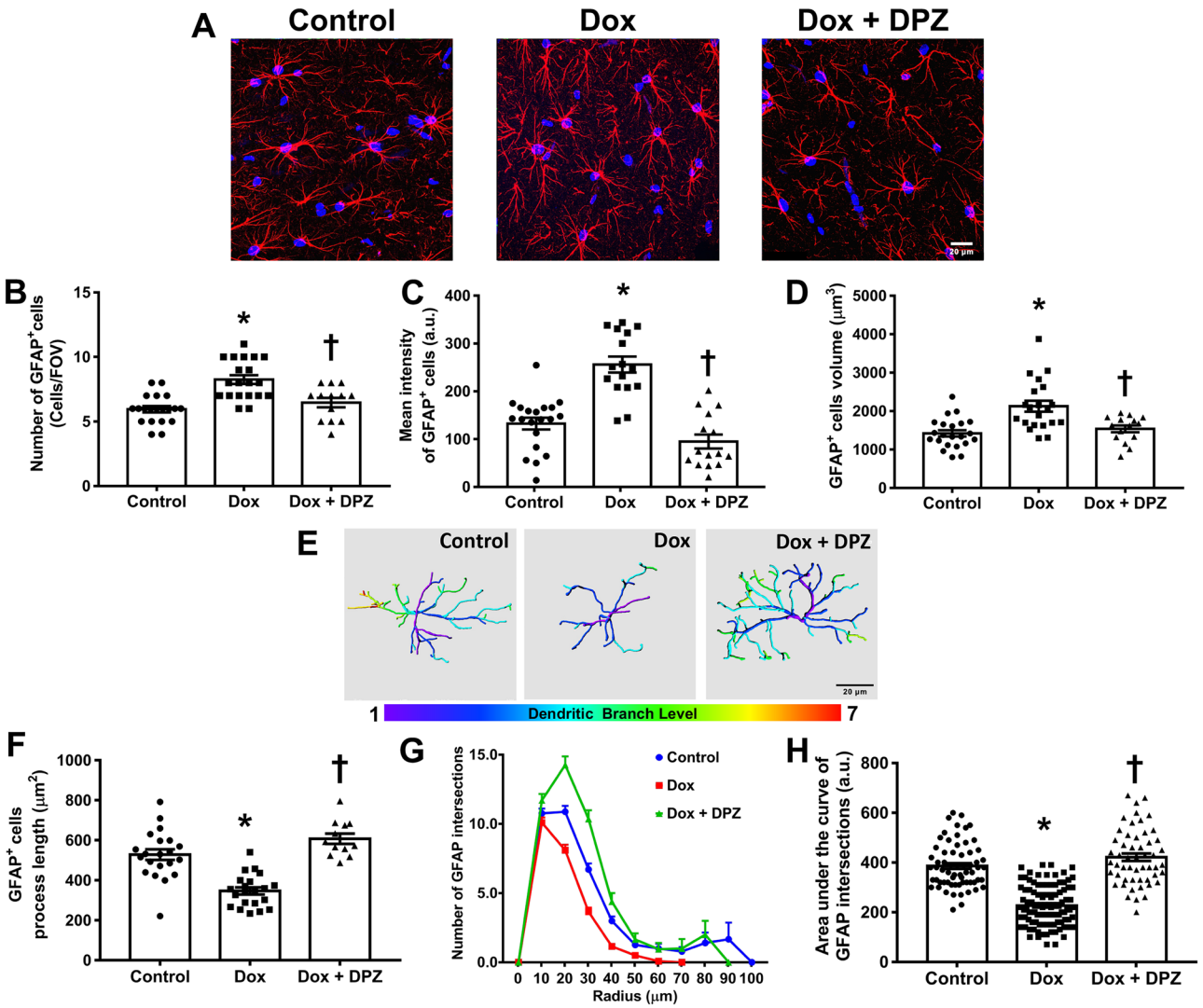

Fig. 4 The effects of donepezil on astrocyte morphology in rats with doxorubicin-induced chemobrain. **A** Representative images of GFAP immunofluorescence under confocal microscopy at CA1 of the hippocampus. **B** The number of GFAP positive cells. **C** Mean intensity of GFAP positive cells. **D** Soma volume of GFAP positive cells. **E** Representative branch level of astrocyte processes. **F** Process length of GFAP positive cells. **G** Astrocyte process complexity as the number of GFAP positive cell process intersections using Sholl analysis. H Representative area under the curve of Sholl analysis. $n = 12$ slices from 6 rats/group; * $p < 0.05$ vs. Control; † $p < 0.05$ vs. Dox (one-way ANOVA followed by an LSD post hoc test); Dox, doxorubicin; DPZ, donepezil; FOV, field of vision

exhibited a significantly higher expression level of BACE enzyme than that of the control group ($p < 0.05$; Fig. 6a and c). Dox administration also induced the hyperphosphorylation of Tau protein as represented by a substantial increase in the expression ratio of phosphorylated Tau (p-Tau) to a total form of Tau, compared with the control group ($p < 0.05$; Fig. 6a and d). In addition to AD proteins, a significant increase in the protein RAGE was observed in the Dox group, compared to that observed in the control group ($p < 0.05$; Fig. 6e). DPZ treatment effectively reduced the expression of both AD-related proteins and the aging marker to levels equivalent to the control group ($p < 0.05$; Fig. 6a–e).

We also investigated alterations in neurotrophic factors and cell differentiation in the hippocampus. In comparison to the control group, Dox-treated rats exhibited a significant decline in the expression level of BDNF ($p < 0.05$; Fig. 6a and f). Dox administration downregulated the activation of TrkB as shown by a substantial decrease in the ratio of phosphorylated TrkB at Tyrosine 515 to a total form of TrkB (p-TrkB^{Tyr515}/TrkB) ($p < 0.05$; Fig. 6a and g). The hippocampal expression of DCX was also significantly lower in the Dox group than in the control group ($p < 0.05$; Fig. 6a and h). Notably, DPZ treatment restored signaling of neurogenesis by enhancing the level of BDNF and the p-TrkB^{Tyr515}/TrkB expression ratio ($p < 0.05$; Fig. 6a and f–h).

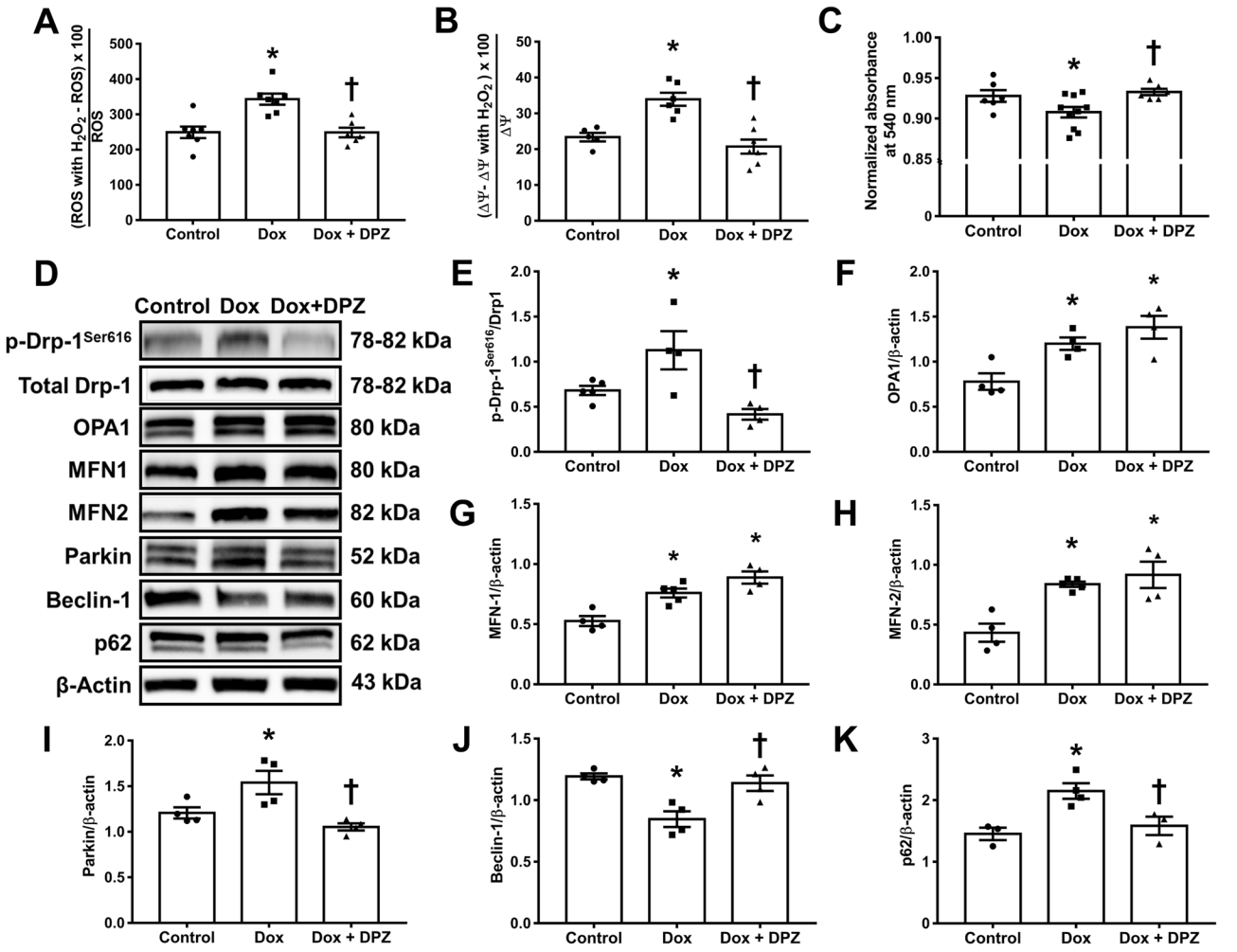

Fig. 5 The effects of donepezil on brain mitochondrial function, hippocampal mitochondrial dynamics, mitophagy, and autophagy in rats with doxorubicin-induced chemobrain. **A** The percentage change of mitochondrial ROS level stimulated with H_2O_2. **B** Brain mitochondrial membrane potential changes after H_2O_2 stimulation. **C** Mitochondrial swelling as indicated by absorbance at a wavelength of 540 nm. **D** Representative western blot bands. **E** The expression ratio of p-Drp-1^{Ser616}/Drp-1. **F** OPA1 protein expression. **G** MFN-1 protein expression. **H** MFN-2 protein expression. **I** Parkin protein expression. **J** Beclin-1 protein expression. **K** p62 protein expression. $n = 5–8$/group for mitochondrial function and $n = 3–5$/group for western blotting; * $p < 0.05$ vs. Control; † $p < 0.05$ vs. Dox (one-way ANOVA followed by an LSD post hoc test). ΔΨ, mitochondrial membrane potential; Dox, doxorubicin; DPZ, donepezil; Drp-1, dynamin-related protein-1; p-Drp-1^{Ser616}, phosphorylated dynamin-related protein-1 at serine 616; MFN-1, mitofusin-1; MFN-2, mitofusin-2; OPA1, optic atrophy 1; ROS, reactive oxygen species

DPZ Mitigated Dendritic Spine Loss and Neuronal Cell Death Against Dox-Induced Neurotoxicity Through the Inhibition of Apoptosis and Necroptosis

Dox administration significantly decreased the density and volume of dendritic spines compared with those observed in the control group ($p < 0.05$; Fig. 7a–c). However, DPZ effectively preserved the dendritic spine number and spine volume in comparison to the Dox group ($p < 0.05$; Fig. 7a–c). Adding weight to these findings, the expression of the postsynaptic density protein 95 (PSD95) in the Dox group was lower than in the control group but was subsequently restored to a level equal to that of the control group following treatment with DPZ ($p < 0.05$; Fig. 7d and e). In addition, the expression levels of Bax/Bcl-2 and cleaved caspase-3/caspase-3 were dramatically increased in the Dox group when compared with the control group, indicating an increase in neuronal apoptosis ($p < 0.05$; Fig. 7d and f). DPZ treatment significantly reduced Bax/Bcl-2 and cleaved caspase-3/caspase-3 ratios in comparison to Dox-treated rats ($p < 0.05$; Fig. 7d and g). We demonstrated, for the first time, that Dox-induced neuronal death involved necroptosis, as indicated by substantial increases in the expression levels of p-RIP-1/RIP-1 and p-MLKL/MLKL ($p < 0.05$; Fig. 7d, h, and i). This expression of necroptotic proteins was significant decreased in the

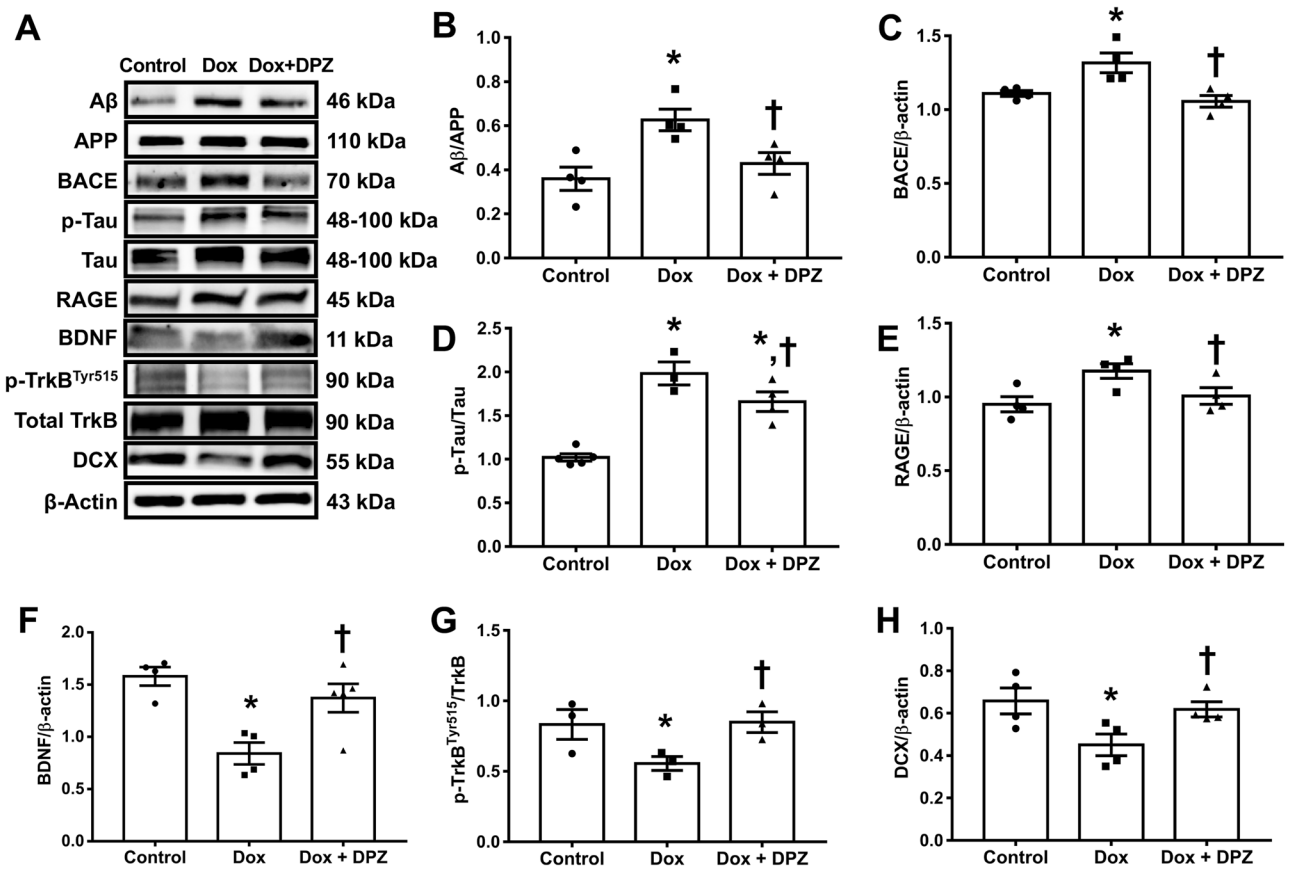

Fig. 6 The effects of donepezil on formation of AD-related proteins, brain aging, and neurogenesis in the hippocampus of rats with doxorubicin-induced chemobrain. **A** Representative western blot bands. **B** The expression ratio of amyloid-β/APP. **C** BACE protein expression. **D** The expression ratio of p-Tau/Tau. **E** RAGE protein expression. **F** BDNF protein expression. **G** The expression ratio of p-TrkB^{Tyr515}/TrkB. **H** DCX protein expression. $n = 3$–5/group; * $p < 0.05$ vs. Control; † $p < 0.05$ vs. Dox (one-way ANOVA followed by an LSD post hoc test). APP, amyloid precursor protein; BACE, β-site amyloid precursor protein cleaving enzyme; BDNF, brain-derived neurotrophic factor; DCX, doublecortin; Dox, doxorubicin; DPZ, donepezil; TrkB, tropomyosin receptor kinase B; p-TrkB^{Tyr515}, phosphorylated TrkB at tyrosine 515; RAGE, receptor for advanced glycation end products

Dox + DPZ group, compared to the Dox group ($p < 0.05$; Fig. 7d, h, and i). Collectively, Dox administration induced both apoptotic and necroptotic cell death in the hippocampus which was attenuated by DPZ treatment.

DPZ Did Not Interfere with the Response of Dox Treatment in Breast Cancer Cells

To assess the feasibility of the practical clinical use of DPZ treatment in cancer patients, we investigated the influence of DPZ on the anti-tumor efficacy of Dox against breast cancer cell lines. Our results showed that DPZ in all tested concentrations did not influence the cell viability of MCF-7 and MDA-MB-231 cells. Dox at a concentration of 0.3125 μM significantly reduced the cell viability of both cell lines, and these results were not adversely affected by co-treatment with DPZ. These findings reinforce the prospect of using DPZ in a clinical setting (Fig. 8a and b).

Discussion

Chemobrain has been identified as the most common neurological consequence following chemotherapy across numerous populations of cancer patients [7]. However, there is currently no available intervention proven to alleviate chemobrain. Therefore, we sought to determine the efficacy of AChE inhibition in improving cognition and various aspects of neuropathology in rats with Dox-induced chemobrain. Our results highlighted that inhibition of AChE exerted neuroprotective effects against Dox-induced chemobrain as follows: (i) improvement of long-term learning and memory; (ii) attenuation of neuroinflammation and brain oxidative stress; (iii) restoration of mitochondrial homeostasis and balancing of mitophagy and autophagy; (iv) protection of AD-related protein formation and aging acceleration; (v) enhancement of neurogenesis; (vi) mitigation of glial activation; and (vii) inhibition of apoptosis and necroptosis.

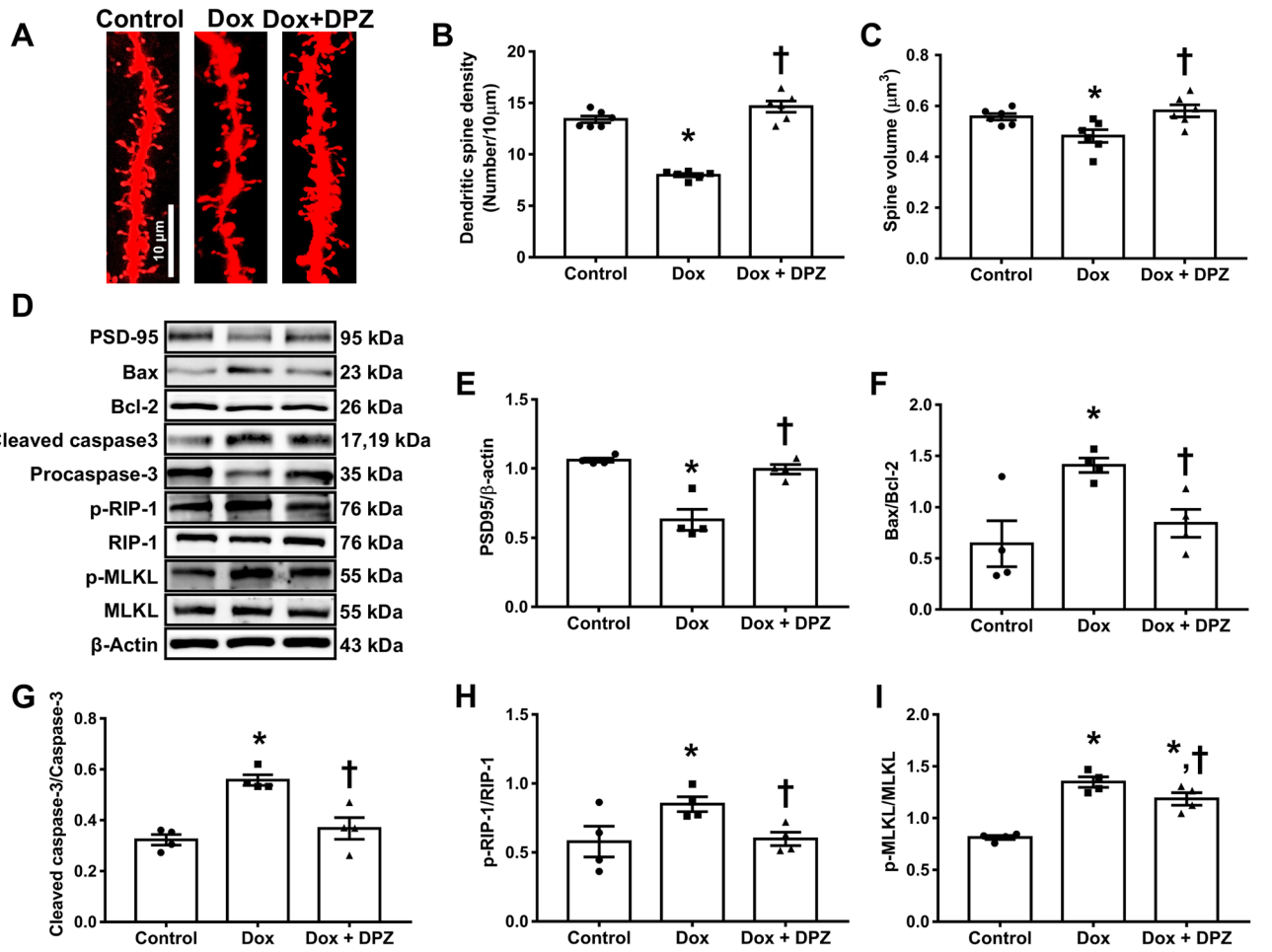

Fig. 7 The effects of donepezil on dendritic spine density and hippocampal cell death in rats with doxorubicin-induced chemobrain. **A** Representative images of dendritic spine density using DiI staining. **B** The number of dendritic spines per 10 µm apical tertiary dendrite. **C** Dendritic spine volume. **D** Representative western blot bands. **E** PSD95 expression level. **F** The expression ratio of Bax/Bcl-2. **G** The expression ratio of cleaved caspase-3/caspase-3. **H** The expression ratio of p-MLKL/MLKL. I The expression ratio of p-RIP-1/RIP1. $n = 12$ slices from 6 rats/group for DiI staining and $n = 3$–5/group for western blotting; * $p < 0.05$ vs. Control; † $p < 0.05$ vs. Dox (one-way ANOVA followed by an LSD post hoc test); Dox, doxorubicin; DPZ, donepezil; PSD95, postsynaptic density protein 95

We also found evidence to suggest that treatment with DPZ does not alter the anti-cancer properties of Dox in two phenotypes of breast cancer.

In this study, modified NOL following by NOR tasks were performed to assess long-term cognitive function. Dox-treated rats exhibited an apparent impairment in

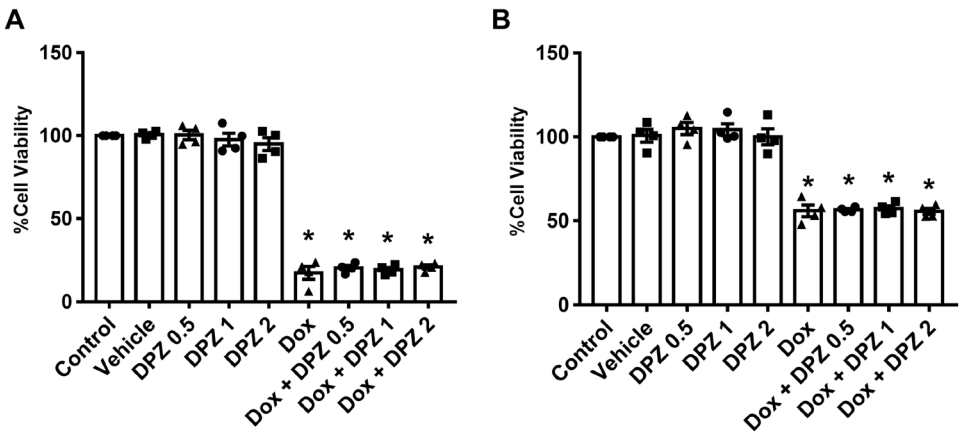

Fig. 8 The effects of donepezil on anti-cancer effects of doxorubicin treatment in MCF-7 and MDA-MB-231 breast cancer cell lines. **A** % cell viability of MCF-7 cells. **B** % cell viability of MDA-MB-231. $n = 4$ biological replicates; * $p < 0.05$ vs. Control (one-way ANOVA followed by an LSD post hoc test)

spatial learning and memory as manifested by a decreased preference index in NOL and NOR phases, while Dox administration did not affect either locomotion or anxiety level. These results confirmed the rigor of our modified cognitive testing procedure which placed a cognitive load on long-term memory involving the hippocampus. Our results demonstrate that Dox impaired long-term learning and memory without impacting locomotion or causing anxiety-like behavior. Findings consistent with previous studies showed that Dox injection disrupted performance in the Morris water maze test, indicating the dysfunction of hippocampal-dependent spatial ability [14, 33]. These corroborate the clinical report of a substantially lower volume of the left hippocampus, together with the impairment of verbal memory which has been observed in breast cancer survivors [34].

Previous studies have shown that treatment with Dox increased the level of circulating TNF-α capable of crossing the BBB which can further amplify the inflammatory signals via the translocation of NF-κB transcriptional factor, resulting in local massive production of pro-inflammatory cytokines and ROS/RNS-producing enzymes from glial cells in the brain [11, 12, 35]. Various pieces of research have revealed a profound relationship between the phenotype of microglia and astrocytes in neurodegenerative disorders [36, 37]. The microglia and astrocytes are traditionally dichotomized into the neurotoxic phenotype (M1 microglia and A1 astrocytes) and the neuroprotective phenotype (M2 microglia and A2 astrocytes), characterized by amoeboid and ramified morphologies, respectively [37]. Previous models of Dox-induced chemobrain have measured only the number of positive cells and/or arbitrary units of glial marker intensity [10–12, 38, 39]. However, this alteration of glial parameters may not be sufficient to reflect the actual status of glial activation effected by Dox administration. Here, we showed corroborative evidence regarding the morphological changes of microglia and astrocyte following Dox treatment in various aspects. Dox administration increased the number, fluorescence intensity, and soma volume of Iba-1 and GFAP positive cells. In addition, a decline in process length and filament complexity of Iba-1 and GFAP positive cells was detected in the CA1 area of Dox-treated rats. Given that an increase in the complexity of astrocyte ramifications was recognized as the major hallmark of astrogliosis in particular to response to stroke [40], traumatic brain injury [40], and focal penetrating lesion [41]. The hypertrophic morphology of reactive astrocyte observed in these insults was shown to play a critical role in restricting a damaged area and protecting neural tissue following focal brain injuries [42]. However, there are several types of astrogliosis or astrocyte reactivity. A hypertrophic astrocyte with increased ramifications is one of several phenotypes observed in those states [43]. Indeed, the shapeshifting of reactive astrocytes morphology depends on the severity and nature of pathological conditions. The transcriptomic analysis has demonstrated that LPS-induced neuroinflammation and MCAO-induced brain ischemia showed two distinctly different subtypes of reactive astrocytes [44], further confirming the highly heterogeneity of reactive astrocyte states. In terms of our study, it has been commonly known that Dox caused cognitive decline by creating chronic neuroinflammatory environment in the brain through the activation of microglia which is rather similar with the aforementioned LPS-exposed model. This is also supported by a previous study which showed that activated microglia can trigger the reactivity of astrocyte into A1 harmful phenotype as represented by a decrease in number of branches and complexity score, together with an upregulated A1-specific gene expression [45]. This A1 phenotype of reactive astrocyte can also promote neuronal death which possibly lead to cognitive impairment in several neurodegenerative diseases [45]. Additionally, a loss of astrocyte arborization has also been reported in several models such as Alzheimer's disease [46] and amyotrophic lateral sclerosis [47], further indicating that a decreased complexity of astrocyte is involved with the pathogenesis of several neurodegenerative diseases. In terms of microglial morphological changes, our group has demonstrated that peripheral inflammatory insult caused by high-fat diet can induce the activation the reactivity of microglia into an amoeboid-shaped phenotype as shown by decreased ramification and increased soma volume [26]. This microglial morphology has been recognized as a neurotoxic M1 phenotype which is able to release pro-inflammatory cytokines in response to both peripheral and brain inflammatory insults [45, 48, 49].

Collectively, we suggested that Dox caused peripheral inflammation which subsequently induced the activation of microglia in the brain, resulting in a polarization of microglia into the ameboid-shaped neurotoxic phenotypes and a release of pro-inflammatory cytokines TNF-α and IL-6. These cytokines can further provoke the reactivity of astrocyte toward neurotoxic states which leads to loss of their physiological function, neuronal death, and ultimately cognitive decline in a model of Dox-induced chemobrain. Our findings of increased TNF-α and IL-6 are consistent with the previous body of clinical research that demonstrates that elevated levels of serum TNF-α and IL-6 are associated with impairment of verbal memory performance and reduced left hippocampal volume in breast cancer patients [34]. These findings support the critical role of pro-inflammatory cytokines in the cognitive deficits following breast cancer treatment with chemotherapy.

There is also evidence that shows TNF-α to be a potential causal mediator in mitochondrial damage following Dox administration [15, 16]. Park et al. showed that multiple injections of Dox impaired mitochondrial calcium retention

capacity and increased mitochondrial H_2O_2 levels in the hippocampus [14]. Adding weight to these findings, we demonstrated that brain mitochondria from the Dox group lost their neutralizing ability to control oxidative stress mimicked by H_2O_2 incubation. Therefore, brain mitochondria can no longer sustain membrane potential and permeability, resulting in mitochondrial membrane depolarization and subsequent mitochondrial swelling. Mitochondrial dysfunction and the activation of glial cells could contribute to the aggravation of brain oxidative stress as indicated by increased brain MDA level in Dox-treated rats. Also, the compensative upregulation of GPx4 was observed in the hippocampus of Dox-treated rats, providing unmet antioxidant capacity against oxidative stress due to no adaptive expression of SOD2 (main antioxidant enzyme against superoxide radicals). These data might explain the persistent brain oxidative burst detected in this study. In the physiological condition, mitochondria possess a morphological adaptation to rescue damaged units and to respond in cellular stress conditions. This process is called mitochondrial dynamics which is regulated by an equal balance between fusion and fission machinery [50, 51]. Our results showed for the first time that Dox possibly disturbed mitochondrial dynamics in the hippocampus. Treatment with Dox increased the expression ratio of p-Drp-1^{ser616}/Drp-1, indicating excessive mitochondrial fission. Increased phosphorylation of Drp-1 at the serine616 residues in postmortem brain of AD patients was suspected as the possible mechanism of neuronal dysfunction, showing a connection with neurological disorders [52]. Notably, mitochondrial fusion was enhanced by Dox administration, as demonstrated by increased expressions of MFN1, MFN2, and OPA1. We speculate that this process compensated against Dox-mediated oxidative stress and mitochondrial damage.

Subsequently, mitophagy and autophagy are also important mechanisms involved in the clearance and turnover of dysfunctional mitochondria by a fission process through lysosomal degradation [53]. Pertinent to this, Dox enhanced mitophagy as represented by increased Parkin expression. The disruption of autophagy was observed in Dox-treated rats. These results suggested that brain mitochondria underwent mitophagy by Parkin-dependent ubiquitination in response to Dox administration; however, these mitochondria were unable to be degraded because of a disturbance of autophagic events.

An interplay between neuroinflammation and glial activation has been identified as a major hallmark underlying dementia, particularly AD. Alongside these findings, the amyloid hypothesis and tauopathy are accepted as key features governing the pathology of AD [54, 55]. We showed for the first time that Dox administration upregulated the expression of BACE-1, a potent enzyme responsible for the initial cleavage of the APP to generate Aβ, resulting in the increased formation of Aβ in the hippocampus of Dox-treated rats. Indeed, it has been shown that the inflammatory cytokines released from activated microglia and astrocytes potentially enhanced the activity of BACE and production of Aβ which could further bind with RAGE, resulting in brain oxidative bursts and mitochondrial dysfunction via the activation of NF-κB [56]. Correlated with clinical reports, patients with primary breast cancer who underwent chemotherapy exhibited a higher Alzheimer's disease probability compared to subjects who received no chemotherapy [57, 58]. Defective mitochondria have been considered as being a driver of AD and tauopathy [59]. We demonstrated that Dox also induced the phosphorylation of Tau, together with an increased level of the aging marker RAGE. In support of our findings, chemotherapy has been shown to induce the activation of astrocytes, resulting in the acceleration of the development of brain aging represented by the accumulation of tau clustering and loss of synaptic integrity [60].

Of note, some long-standing evidence has also reported that glial activation has impact on the modulation of hippocampal neurogenesis. These initial works demonstrated that microglial activation following LPS administration decreased the release of BDNF in the hippocampus, leading to impaired neurogenesis [61, 62]. Similarly, TNF-α directly reduced the differentiation of hippocampal neural precursor cells (NPCs) into newly formed neurons, while increasing the development of astrocytes through the upregulation of the anti-neurogenic *Hes1* gene. The reduction of BDNF and TrkB, together with DCX positive neuronal progenitors, is likely to be affected by dysfunctional hippocampal mitochondria and is partly responsible for the impairment of hippocampal-dependent learning and memory in the Dox-induced chemobrain model [14]. Consistent with these results, we observed decreased markers of neurogenesis in response to Dox administration, suggesting that Dox disrupted hippocampal neurogenesis via glial activation and brain mitochondrial dysfunction.

Our investigation discovered dysplasticity in response to Dox treatment, indicated by loss of dendritic spine density and volume, together with the reduction of the postsynaptic protein marker PSD-95. Previous studies demonstrated that inflammatory mediators released from activated microglia also antagonized the stimulatory BDNF signaling and induced excitotoxicity through the activation of AMPA receptors, thereby contributing to dendritic spine damage [63]. In addition, oxidative stress in the brain causes cognitive deficits by disrupting dendritic spine formation [64]. As expected, Dox-induced hippocampal apoptosis demonstrated an increased expression ratio of Bax/Bcl-2 and cleaved caspase-3/procaspase-3. These findings were supported by the binding of TNF-α with TNFR1 and dysfunctional

mitochondria, which may have initiated the apoptotic cascade by opening mPTPs and releasing cytochrome *c* after a Dox injection as found in a previous report [14]. Importantly, we showed for the first time that Dox also exacerbated neuronal cell death in the hippocampus via necroptosis as confirmed by increased activation of RIP-1 and MLKL via phosphorylation. It is therefore possible that the Dox-mediated TNF-α elevation could trigger the induction of the RIPK1–RIPK3–MLKL axis by the ligation with TNFR1, culminating in the formation of necrosomes and causing necroptosis-dependent neuronal death [65].

ACh is a neurotransmitter in the cholinergic nervous system and is crucial for memory formation via long-term potentiation (LTP) enhancement [66]. Unfortunately, Dox-induced oxidative stress enhances the ROS-mediated activity of AChE and depletes choline content in the brain [11, 67]. Cholinergic activation using DPZ, however, has recently been shown to improve various cognitive aspects in models of chemobrain [68, 69]. Consistent with these reports, DPZ co-treatment in our study restored cognitive function in Dox-treated rats, resulting in outstanding protective cholinergic enhancement against cognitive impairment in Dox-treated rats. Conceptually, DPZ co-treatment potentially attenuated the reactivity of microglia and astrocytes toward a neurotoxic state, suppressing TNF-α and IL-6 mRNA expressions. These findings signified the favorable effect of DPZ on glial activation against Dox-induced neuroinflammation. These data are supported by a study demonstrating that DPZ directly reduced the release of pro-inflammatory cytokines in LPS-treated microglia by repressing NF-κB signaling in an ACh- and nAChRs-independent manner [70]. Furthermore, a considerable body of clinical research in AD patients showed that DPZ exerts both potent antioxidant and anti-inflammatory effects through immunological modulation of the cholinergic anti-inflammatory reflex [71]. It is thus plausible to consider whether an increase in ACh by DPZ treatment ligands with the α7-nicotinic acetylcholine receptor (α7nAChR) in turn inhibits the translocation of NF-κB through a JAK2–STAT3 activation, thereby reducing the production of TNF-α from cytokine-producing macrophages [72]. Therefore, it is most likely that the neuroprotective effects of DPZ against Dox-induced cognitive decline are mediated through the attenuating effect of DPZ itself on glial cells and the inhibition of TNF-α production in the periphery.

Importantly, DPZ co-treatment restored all brain mitochondrial status and preserved the balance of mitophagy and autophagy in the hippocampus of rats with Dox-induced chemobrain. Although the precise mechanism used by DPZ in protecting against brain mitochondrial dysfunction has still not been clearly elucidated, it has been previously shown that genetic ablation of TNF-α or the administration of neutralizing antibodies against TNF-α abrogated doxorubicin-induced mitochondrial dysfunction [15, 16]. DPZ has also been shown to prevent mitochondrial dysfunction by directly reducing the accumulation of amyloid-β in the brain mitochondria of AD mice via a cholinergic-independent manner [73]. Taken all these findings together, we predicted that DPZ would provide benefits in mitochondrial homeostasis partly by suppressing peripheral and brain TNF-α production and causing the reduction of amyloid-β production in Dox-treated rats. DPZ mitigated alterations of neurogenesis signaling and neuronal differentiation in the hippocampus of Dox-treated rats. Our results added further weight to the earlier findings, which indicated that intervention with DPZ enhanced neurogenesis through the stimulation of α7 nicotinic acetylcholine receptor (α7nAChR) [74]. α7 nAChR mediated neurogenesis by allowing calcium influx which in turn leads to CREB phosphorylation and initiates BDNF transcription [74].

We observed a marked increase in the density of dendritic spines in the CA1 subregion of rats co-treated with DPZ. We speculated that DPZ sustained synaptic integrity in rats with chemobrain through alleviating oxidative stress and glial activation. DPZ co-treatment exerted an influential anti-apoptotic property in Dox-induced chemobrain, suggesting DPZ preserved neuronal survival by attenuating mitochondrial dysfunction and brain inflammation. Indeed, ACh elevated by DPZ treatment could activate α7nAChRs which also instigates the survival PI3K-Akt-Bcl-2 pathway [75], leading to the neuroprotection against Dox toxicity found in the present study. Unfortunately, there is still a lack of knowledge regarding the anti-necroptotic effects of DPZ in the brain. We suggest that it could be due to the suppressed expression of TNF-α, thereby making TNFR1 unable to initiate the signaling transduction of the necroptosis pathway. The proposed neuroprotective mechanisms of donepezil against Dox-induced chemobrain are summarized and shown in Fig. 9.

In conclusion, the major findings of this study are that Dox impaired long-term learning and memory through brain lesions caused by brain oxidative stress, brain mitochondrial dysfunction, and neuroinflammation by glial activation. It also contributed to an accumulation of AD-related proteins, aging acceleration, a decline of neurogenesis, loss of dendritic spines, and subsequent neuronal death through both apoptosis and necroptosis. The inhibition of AChE using DPZ exerted neuroprotective effects measurable by improvement in cognition and restoration of all aforementioned pathologies against Dox-induced chemobrain without interfering with the anti-cancer activity of Dox. This study illustrates the potential therapeutic advantages of the AChE inhibitor (DPZ) as a promising novel treatment to protect against neurological sequelae in cancer patients.

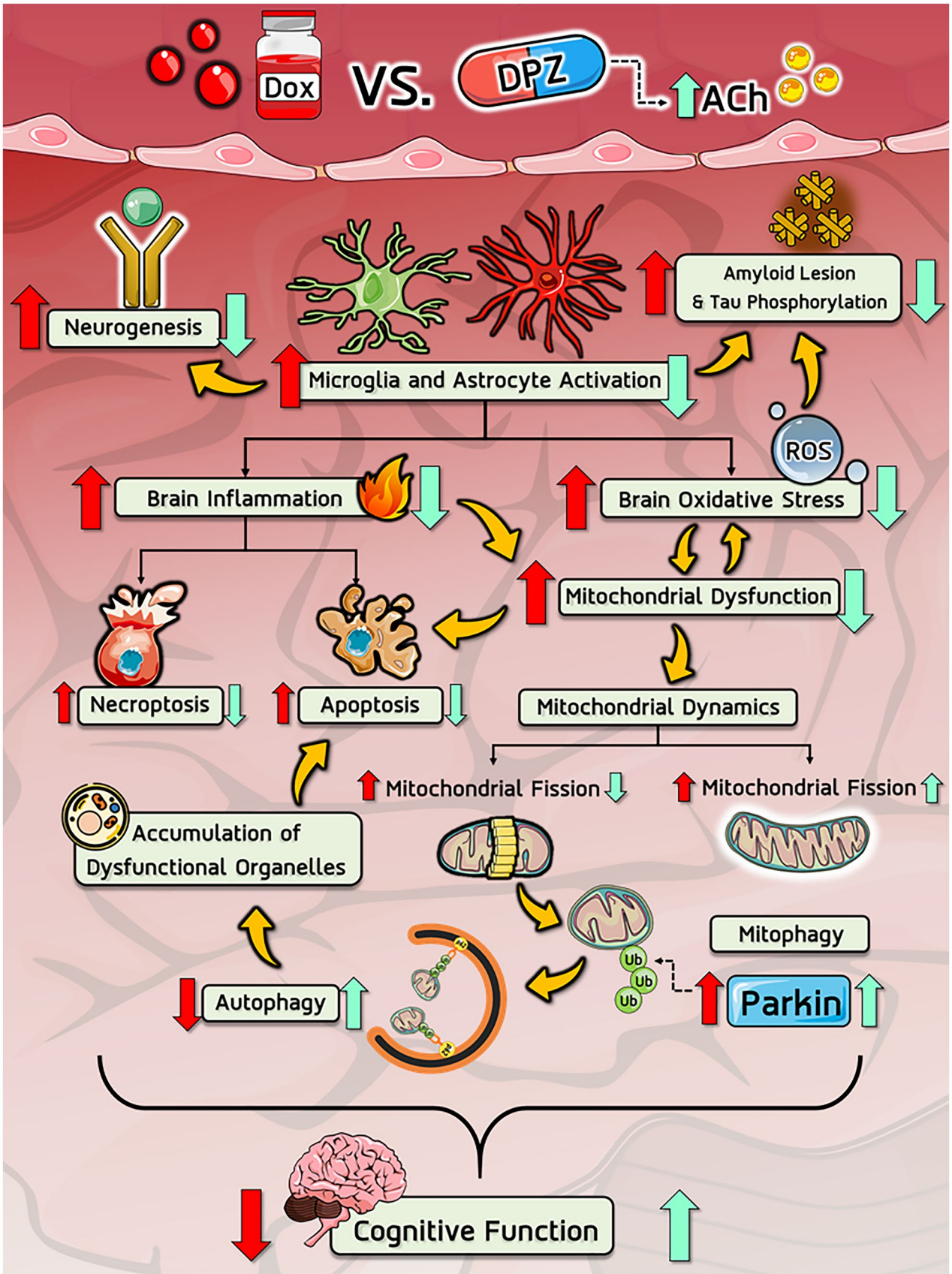
Dox
VS.
DPZ
ACh
Neurogenesis
Amyloid Lesion
& Tau Phosphorylation
Microglia and Astrocyte Activation
ROS
Brain Inflammation
Brain Oxidative Stress
Mitochondrial Dysfunction
Necroptosis
Apoptosis
Mitochondrial Dynamics
Mitochondrial Fission
Mitochondrial Fission
Accumulation of
Dysfunctional Organelles
Mitophagy
Ub
Ub
Ub
Parkin
Autophagy
Cognitive Function

◂**Fig. 9** The neuroprotective effects of donepezil against doxorubicin-induced chemobrain. Dox treatment induced the activation of microglia and astrocytes which in turn caused neuroinflammation and brain oxidative stress. Dox-mediated glial activation and brain oxidative stress also contributed to the disruption of hippocampal neurogenesis and the promotion of AD and tauopathy lesions. Oxidative stress weakened mitochondrial function and altered mitochondrial homeostasis including mitochondrial dynamics and the process of mitochondrial degradation, resulting in the accumulation of damaged cellular organelles. Elevated inflammatory cytokines and accumulated dysfunctional mitochondria potentiated neuronal apoptosis. TNF-α also initiated necroptosis in the hippocampus. All of these pathologies orchestrated the impairment of cognitive function in rats with Dox-induced chemobrain. However, co-treatment with DPZ exerted potent neuroprotection by increasing systemic and brain ACh, eventually culminating in the improvement of cognitive function and the restoration of the aforementioned pathological events in Dox-treated rats. Red arrows represent the effects of Dox treatment and Green arrows represent the impact of intervention with DPZ in the chemobrain model. ACh, acetylcholine; Dox; Dox, doxorubicin; DPZ, donepezil; Ub, ubiquitin

Supplementary Information The online version contains supplementary material available at https://doi.org/10.1007/s13311-021-01092-9.

Acknowledgements We would like to thank Dillon Prus for his language editing and proofreading of this manuscript.

Required Author Forms Disclosure forms provided by the authors are available with the online version of this article.

Funding This work was supported by a Senior Research Scholar grant from the National Research Council of Thailand (SCC); the Royal Golden Jubilee Ph.D. program (PHD/0106/2561 BO&SCC); an NSTDA Research Chair Grant from the National Science and Technology Development Agency Thailand (NC); and a Chiang Mai University Excellence Center Award (NC).

Declarations

Conflict of Interest The authors declare no competing interests.

References

1. Siegel RL, Miller KD, Jemal A. Cancer statistics, 2018. CA Cancer J Clin. 2018;68:7-30.
2. Miller KD, Siegel RL, Lin CC, Mariotto AB, Kramer JL, Rowland JH, et al. Cancer treatment and survivorship statistics, 2016. CA Cancer J Clin. 2016;66:271-89.
3. Zandbergen N, de Rooij BH, Vos MC, Pijnenborg JMA, Boll D, Kruitwagen R, et al. Changes in health-related quality of life among gynecologic cancer survivors during the two years after initial treatment: a longitudinal analysis. Acta Oncol. 2019:1–11.
4. Brezden CB, Phillips KA, Abdolell M, Bunston T, Tannock IF. Cognitive function in breast cancer patients receiving adjuvant chemotherapy. J Clin Oncol. 2000;18:2695-701.
5. van Dam FS, Schagen SB, Muller MJ, Boogerd W, vd Wall E, Droogleever Fortuyn ME, et al. Impairment of cognitive function in women receiving adjuvant treatment for high-risk breast cancer: high-dose versus standard-dose chemotherapy. J Natl Cancer Inst. 1998;90:210–8.
6. Ongnok B, Chattipakorn N, Chattipakorn SC. Doxorubicin and cisplatin induced cognitive impairment: The possible mechanisms and interventions. Exp Neuro. 2020;324:113118.
7. Ahles TA, Saykin AJ. Candidate mechanisms for chemotherapy-induced cognitive changes. Nat Rev Cancer. 2007;7:192-201.
8. Wang XM, Walitt B, Saligan L, Tiwari AF, Cheung CW, Zhang ZJ. Chemobrain: a critical review and causal hypothesis of link between cytokines and epigenetic reprogramming associated with chemotherapy. Cytokine. 2015;72:86-96.
9. Correa DD, Ahles TA. Cognitive adverse effects of chemotherapy in breast cancer patients. Curr Opin Support Palliat Care. 2007;1:57-62.
10. Leung W-S, Kuo W-W, Ju D-T, Wang T-D, Shao-Tsu Chen W, Ho T-J, et al. Protective effects of diallyl trisulfide (DATS) against doxorubicin-induced inflammation and oxidative stress in the brain of rats. Free Radic Biol Med. 2020;160:141-8.
11. El-Agamy SE, Abdel-Aziz AK, Wahdan S, Esmat A, Azab SS. Astaxanthin Ameliorates Doxorubicin-Induced Cognitive Impairment (Chemobrain) in Experimental Rat Model: Impact on Oxidative, Inflammatory, and Apoptotic Machineries. Mol Neurobiol. 2018;55:5727-40.
12. Allen BD, Apodaca LA, Syage AR, Markarian M, Baddour AAD, Minasyan H, et al. Attenuation of neuroinflammation reverses Adriamycin-induced cognitive impairments. Acta Neuropathol Commun. 2019;7:186.
13. Monzio Compagnoni G, Di Fonzo A, Corti S, Comi GP, Bresolin N, Masliah E. The Role of Mitochondria in Neurodegenerative Diseases: the Lesson from Alzheimer's Disease and Parkinson's Disease. Mol Neurobiol. 2020;57:2959-80.
14. Park HS, Kim CJ, Kwak HB, No MH, Heo JW, Kim TW. Physical exercise prevents cognitive impairment by enhancing hippocampal neuroplasticity and mitochondrial function in doxorubicin-induced chemobrain. Neuropharmacology. 2018;133:451-61.
15. Ren X, Keeney JTR, Miriyala S, Noel T, Powell DK, Chaiswing L, et al. The triangle of death of neurons: Oxidative damage, mitochondrial dysfunction, and loss of choline-containing biomolecules in brains of mice treated with doxorubicin. Advanced insights into mechanisms of chemotherapy induced cognitive impairment ("chemobrain") involving TNF-α. Free Radic Biol Med. 2019;134:1–8.
16. Tangpong J, Cole MP, Sultana R, Joshi G, Estus S, Vore M, et al. Adriamycin-induced, TNF-alpha-mediated central nervous system toxicity. Neurobiol Dis. 2006;23:127-39.
17. Kohman RA, Rhodes JS. Neurogenesis, inflammation and behavior. Brain Behav Immun. 2013;27:22-32.
18. Dietrich J, Prust M, Kaiser J. Chemotherapy, cognitive impairment and hippocampal toxicity. Neuroscience. 2015;309:224-32.
19. Kim SH, Kandiah N, Hsu J-L, Suthisisang C, Udommongkol C, Dash A. Beyond symptomatic effects: potential of donepezil as a neuroprotective agent and disease modifier in Alzheimer's disease. Br J Pharmacol. 2017;174:4224-32.
20. Blennow K, de Leon MJ, Zetterberg H. Alzheimer's disease. The Lancet. 2006;368:387-403.
21. Ongnok B, Khuanjing T, Chunchai T, Kerdphoo S, Jaiwongkam T, Chattipakorn N, et al. Donepezil provides neuroprotective effects against brain injury and Alzheimer's pathology under conditions of cardiac ischemia/reperfusion injury. Biochimica et Biophysica Acta (BBA) - Molecular Basis of Disease. 2021;1867:165975.
22. Denninger JK, Smith BM, Kirby ED. Novel Object Recognition and Object Location Behavioral Testing in Mice on a Budget. J Vis Exp. 2018.
23. Vogel-Ciernia A, Wood MA. Examining object location and object recognition memory in mice. Curr Protoc Neurosci. 2014;69:8.31.1–17.
24. Candan N, Tuzmen N. Very rapid quantification of malondialdehyde (MDA) in rat brain exposed to lead, aluminium and phenolic antioxidants by high-performance liquid chromatography-fluorescence detection. Neurotoxicology. 2008;29:708-13.

25. Apaijai N, Pintana H, Chattipakorn SC, Chattipakorn N. Effects of vildagliptin versus sitagliptin, on cardiac function, heart rate variability and mitochondrial function in obese insulin-resistant rats. Br J Pharmacol. 2013;169:1048-57.
26. Chunchai T, Thunapong W, Yasom S, Wanchai K, Eaimworawuthikul S, Metzler G, et al. Decreased microglial activation through gut-brain axis by prebiotics, probiotics, or synbiotics effectively restored cognitive function in obese-insulin resistant rats. J Neuroinflammation. 2018;15:11.
27. Sholl DA. Dendritic organization in the neurons of the visual and motor cortices of the cat. J Anat. 1953;87:387-406.
28. Madry C, Kyrargyri V, Arancibia-Carcamo IL, Jolivet R, Kohsaka S, Bryan RM, et al. Microglial Ramification, Surveillance, and Interleukin-1beta Release Are Regulated by the Two-Pore Domain K(+) Channel THIK-1. Neuron. 2018;97:299–312 e6.
29. Chunchai T, Keawtep P, Arinno A, Saiyasit N, Prus D, Apaijai N, et al. N-acetyl cysteine, inulin and the two as a combined therapy ameliorate cognitive decline in testosterone-deprived rats. Aging (Albany NY). 2019;11:3445-62.
30. Pipatpiboon N, Pratchayasakul W, Chattipakorn N, Chattipakorn SC. PPARγ Agonist Improves Neuronal Insulin Receptor Function in Hippocampus and Brain Mitochondria Function in Rats with Insulin Resistance Induced by Long Term High-Fat Diets. Endocrinology. 2012;153:329-38.
31. Pintana H, Apaijai N, Pratchayasakul W, Chattipakorn N, Chattipakorn SC. Effects of metformin on learning and memory behaviors and brain mitochondrial functions in high fat diet induced insulin resistant rats. Life Sci. 2012;91:409-14.
32. Erion JR, Wosiski-Kuhn M, Dey A, Hao S, Davis CL, Pollock NK, et al. Obesity elicits interleukin 1-mediated deficits in hippocampal synaptic plasticity. J Neurosci. 2014;34:2618-31.
33. Lim I, Joung HY, Yu AR, Shim I, Kim JS. PET Evidence of the Effect of Donepezil on Cognitive Performance in an Animal Model of Chemobrain. Biomed Res Int. 2016;2016:6945415.
34. Kesler S, Janelsins M, Koovakkattu D, Palesh O, Mustian K, Morrow G, et al. Reduced hippocampal volume and verbal memory performance associated with interleukin-6 and tumor necrosis factor-alpha levels in chemotherapy-treated breast cancer survivors. Brain Behav Immun. 2013;30 Suppl:S109-16.
35. Aluise CD, Miriyala S, Noel T, Sultana R, Jungsuwadee P, Taylor TJ, et al. 2-Mercaptoethane sulfonate prevents doxorubicin-induced plasma protein oxidation and TNF-α release: Implications for the reactive oxygen species-mediated mechanisms of chemobrain. Free Radical Biology and Medicine. 2011;50:1630-8.
36. Kwon HS, Koh SH. Neuroinflammation in neurodegenerative disorders: the roles of microglia and astrocytes. Transl Neurodegener. 2020;9:42.
37. Franklin H, Clarke BE, Patani R. Astrocytes and microglia in neurodegenerative diseases: Lessons from human in vitro models. Progress in Neurobiology. 2020:101973.
38. El-Derany MO, Noureldein MH. Bone marrow mesenchymal stem cells and their derived exosomes resolve doxorubicin-induced chemobrain: critical role of their miRNA cargo. Stem Cell Res Ther. 2021;12:322.
39. Mohamed RH, Karam RA, Amer MG. Epicatechin attenuates doxorubicin-induced brain toxicity: critical role of TNF-α, iNOS and NF-κB. Brain Res Bull. 2011;86:22-8.
40. Choudhury GR, Ding S. Reactive astrocytes and therapeutic potential in focal ischemic stroke. Neurobiol Dis. 2016;85:234-44.
41. Wilhelmsson U, Bushong EA, Price DL, Smarr BL, Phung V, Terada M, et al. Redefining the concept of reactive astrocytes as cells that remain within their unique domains upon reaction to injury. Proc Natl Acad Sci U S A. 2006;103:17513-8.
42. Myer DJ, Gurkoff GG, Lee SM, Hovda DA, Sofroniew MV. Essential protective roles of reactive astrocytes in traumatic brain injury. Brain. 2006;129:2761-72.
43. Escartin C, Galea E, Lakatos A, O'Callaghan JP, Petzold GC, Serrano-Pozo A, et al. Reactive astrocyte nomenclature, definitions, and future directions. Nat Neurosci. 2021;24:312-25.
44. Zamanian JL, Xu L, Foo LC, Nouri N, Zhou L, Giffard RG, et al. Genomic analysis of reactive astrogliosis. J Neurosci. 2012;32:6391-410.
45. Liddelow SA, Guttenplan KA, Clarke LE, Bennett FC, Bohlen CJ, Schirmer L, et al. Neurotoxic reactive astrocytes are induced by activated microglia. Nature. 2017;541:481-7.
46. Olabarria M, Noristani HN, Verkhratsky A, Rodríguez JJ. Concomitant astroglial atrophy and astrogliosis in a triple transgenic animal model of Alzheimer's disease. Glia. 2010;58:831-8.
47. Rossi D, Brambilla L, Valori CF, Roncoroni C, Crugnola A, Yokota T, et al. Focal degeneration of astrocytes in amyotrophic lateral sclerosis. Cell Death Differ 2008;15:1691-700.
48. Franco R, Fernández-Suárez D. Alternatively activated microglia and macrophages in the central nervous system. Prog Neurobiol. 2015;131:65-86.
49. Süß P, Hoffmann A, Rothe T, Ouyang Z, Baum W, Staszewski O, et al. Chronic Peripheral Inflammation Causes a Region-Specific Myeloid Response in the Central Nervous System. Cell Rep. 2020;30:4082-95.e6.
50. Flippo KH, Strack S. Mitochondrial dynamics in neuronal injury, development and plasticity. J Cell Sci. 2017;130:671-81.
51. Burte F, Carelli V, Chinnery PF, Yu-Wai-Man P. Disturbed mitochondrial dynamics and neurodegenerative disorders. Nat Rev Neurol. 2015;11:11-24.
52. Wang X, Su B, Lee H-g, Li X, Perry G, Smith MA, et al. Impaired balance of mitochondrial fission and fusion in Alzheimer's disease. J Neurosci. 2009;29:9090–103.
53. Fivenson EM, Lautrup S, Sun N, Scheibye-Knudsen M, Stevnsner T, Nilsen H, et al. Mitophagy in neurodegeneration and aging. Neurochem Int. 2017;109:202-9.
54. Cook C, Kang SS, Carlomagno Y, Lin WL, Yue M, Kurti A, et al. Tau deposition drives neuropathological, inflammatory and behavioral abnormalities independently of neuronal loss in a novel mouse model. Hum Mol Genet. 2015;24:6198-212.
55. Zhou X, Li Y, Shi X, Ma C. An overview on therapeutics attenuating amyloid β level in Alzheimer's disease: targeting neurotransmission, inflammation, oxidative stress and enhanced cholesterol levels. Am J Transl Res. 2016;8:246-69.
56. González-Reyes RE, Nava-Mesa MO, Vargas-Sánchez K, Ariza-Salamanca D, Mora-Muñoz L. Involvement of Astrocytes in Alzheimer's Disease from a Neuroinflammatory and Oxidative Stress Perspective. Front Mol Neurosci. 2017;10.
57. Kesler SR, Rao V, Ray WJ, Rao A. Probability of Alzheimer's disease in breast cancer survivors based on gray-matter structural network efficiency. Alzheimers Dement (Amst). 2017;9:67-75.
58. Hosseini SM, Koovakkattu D, Kesler SR. Altered small-world properties of gray matter networks in breast cancer. BMC Neurol. 2012;12:28.
59. Escobar-Khondiker M, Höllerhage M, Muriel M-P, Champy P, Bach A, Depienne C, et al. Annonacin, a natural mitochondrial complex I inhibitor, causes tau pathology in cultured neurons. The Journal of neuroscience : the official journal of the Society for Neuroscience. 2007;27:7827-37.
60. Chiang ACA, Huo X, Kavelaars A, Heijnen CJ. Chemotherapy accelerates age-related development of tauopathy and results in loss of synaptic integrity and cognitive impairment. Brain Behav Immun. 2019;79:319-25.
61. Monje ML, Toda H, Palmer TD. Inflammatory blockade restores adult hippocampal neurogenesis. Science. 2003;302:1760-5.
62. Tanaka S, Ide M, Shibutani T, Ohtaki H, Numazawa S, Shioda S, et al. Lipopolysaccharide-induced microglial activation induces learning and memory deficits without neuronal cell death in rats. J Neurosci Res. 2006;83:557-66.

63. Dorostkar MM, Zou C, Blazquez-Llorca L, Herms J. Analyzing dendritic spine pathology in Alzheimer's disease: problems and opportunities. Acta neuropathologica. 2015;130:1-19.
64. Chugh D, Nilsson P, Afjei SA, Bakochi A, Ekdahl CT. Brain inflammation induces post-synaptic changes during early synapse formation in adult-born hippocampal neurons. Exp Neurol. 2013;250:176-88.
65. Liao S, Apaijai N, Chattipakorn N, Chattipakorn SC. The possible roles of necroptosis during cerebral ischemia and ischemia / reperfusion injury. Arch Biochem Biophys 2020;695:108629.
66. Hasselmo ME. The role of acetylcholine in learning and memory. Curr Opin Neurobiol. 2006;16:710-5.
67. Melo JB, Agostinho P, Oliveira CR. Involvement of oxidative stress in the enhancement of acetylcholinesterase activity induced by amyloid beta-peptide. Neurosci Res. 2003;45:117-27.
68. Lim I, Joung H-Y, Yu AR, Shim I, Kim JS. PET Evidence of the Effect of Donepezil on Cognitive Performance in an Animal Model of Chemobrain. International BR. 2016;2016:6945415-.
69. Winocur G, Binns MA, Tannock I. Donepezil reduces cognitive impairment associated with anti-cancer drugs in a mouse model. Neuropharmacology. 2011;61:1222-8.
70. Hwang J, Hwang H, Lee HW, Suk K. Microglia signaling as a target of donepezil. Neuropharmacology. 2010;58:1122-9.
71. Reale M, Iarlori C, Gambi F, Feliciani C, Isabella L, Gambi D. The acetylcholinesterase inhibitor, Donepezil, regulates a Th2 bias in Alzheimer's disease patients. Neuropharmacology. 2006;50:606-13.
72. Tracey KJ. The inflammatory reflex. Nature. 2002;420:853-9.
73. Ye CY, Lei Y, Tang XC, Zhang HY. Donepezil attenuates Aβ-associated mitochondrial dysfunction and reduces mitochondrial Aβ accumulation in vivo and in vitro. Neuropharmacology. 2015;95:29-36.
74. Shabani Z, Mahmoudi J, Farajdokht F, Sadigh-Eteghad S. An Overview of Nicotinic Cholinergic System Signaling in Neurogenesis. Arch Med Res. 2020;51:287-96.
75. Wallace TL, Porter RH. Targeting the nicotinic alpha7 acetylcholine receptor to enhance cognition in disease. Biochem Pharmacol. 2011;82:891-903.